Charged polycyclic aromatic hydrocarbon clusters and the galactic extended red emission

Young Min Rhee[†], Timothy J. Lee[‡], Murthy S. Gudipati[‡§], Louis J. Allamandola[‡¶], and Martin Head-Gordon[†¶]

[†]Department of Chemistry, University of California, and Chemical Sciences Division, Lawrence Berkeley National Laboratory, Berkeley, CA 94720;
[‡]Astrochemistry Laboratory, National Aeronautics and Space Administration/Ames Research Center, MS 245-6, Moffett Field, CA 94035;
and [§]Institute for Physical Sciences and Technology, University of Maryland, College Park, MD 20742

The species responsible for the broad extended red emission (ERE), discovered in 1975 and now known to be widespread throughout the Galaxy, still is unidentified. Spanning the range from ≈540 to 900 nm, the ERE is a photoluminescent process associated with a wide variety of different interstellar environments. Over the years, a number of plausible candidates have been suggested, but subsequent observations ruled them out. The objects that present the ERE also emit the infrared features attributed to free polycyclic aromatic hydrocarbon (PAH) molecules, suggesting that closely related materials are plausible ERE carriers. Here, we show that the peculiar spectra and unique properties of closed-shell cationic PAH dimers satisfy the existing observational constraints and suggest that emission from mixtures of charged PAH clusters accounts for much of the ERE. This work provides a view into the structures, stabilities, abundances, and ionization balance of PAH-related species in the emission zones, which, in turn, reflects physical conditions in the emission zones and sheds fundamental light on the nanoscale processes involved in carbon-particle nucleation and growth and carbonaceous dust evolution in the interstellar medium.

dimer | excited state | interstellar medium | nanoparticles

The extended red emission (ERE) was discovered in 1975 by Cohen *et al*. (1) in the peculiar object known as the Red Rectangle. Subsequent observations have shown that it is a widespread interstellar photoluminescent phenomenon. Witt and coworkers established that the ERE is associated with reflection nebulae (2, 3), carbon-rich planetary nebulae (4), and the interstellar medium of the Galaxy (5), whereas Darbon, Perrin, Sivan, and coworkers have detected the ERE in galactic HII regions and other galaxies (6–8). A detailed review can be found elsewhere (9).

The ERE is a broad emission band starting near 540 nm that extends into the near infrared (IR). For most objects, the peak wavelength varies between 600 and 700 nm (3), although in the HII region of the Orion nebula, the band seems to peak near 800 nm (8). These variations are thought to arise from modest changes in chemical make-up and differing radiation fields and not from fundamental changes in the nature of the carrier. In some cases, structure appears superposed on the band (10, 11). Over the years a number of possible explanations have been suggested, including photoluminescence from species such as neutral polycyclic aromatic hydrocarbon (PAH) molecules (12), organic residues (13), neutral PAH clusters (14), hydrogenated amorphous carbon particles (15, 16), and silicon nanoparticles (17). Although a carbon-rich carrier was implicated by cosmic abundance constraints, all of these materials have been found wanting in light of subsequent observations. The case for each of these suggestions and the observational difficulties they encounter are summarized nicely by Witt *et al*. (18). Recently, observational constraints have been determined that are especially important in revealing the nature of the carrier. Among these, two are of particular significance. First, the ERE luminescent quantum efficiency is high. With a lower limit on the order of tens of percent (5, 19), the quantum yield could be as high as unity. Second, the ERE process requires initiation with photons between 7.3 and 11.2 eV (18, 20). In a very recent observational tour de force, Witt *et al.* tightened this constraint, making a strong case that the ERE is a two-step process, with the first step involving photons of $E > 10.5$ eV ($\lambda < 118$ nm) to produce the carrier and the second involving UV to visible photons to pump the luminescence from this carrier (18). The first step probably involves photoionization or photodissociation of a preexisting precursor (18).

Although several carbonaceous materials have been rejected, the ubiquity of the ERE and cosmic abundance constraints favor a carbonaceous carrier. Because the ERE is associated with objects that show the mid-IR emission features attributed to free PAH molecules, consideration of unusual PAH-related species as ERE carriers is warranted. Particularly attractive among these are charged PAH clusters. However, because of the experimental inaccessibility of these highly unusual and reactive species, there is no gas phase spectroscopic data available to the best of our knowledge with which to test this hypothesis [PAH dimer cations have been characterized in solution (21, 22) but are subject to strong solvation effects]. To make progress, we explore the spectroscopic properties of various charged PAH clusters by using *ab initio* quantum chemical calculations and show that a unique class of closed-shell charged dimers can account for the ERE.

PAH clusters have been recognized as part of the interstellar PAH model from the outset and are believed to be the self-assembled intermediaries between free gas-phase PAHs and amorphous carbon particles (23). Indeed, Duley *et al.* (24) have explored the spectroscopic and binding properties of various neutral PAH clusters in astrophysical settings. PAH clusters also are produced in sooting flames, for which a separate literature exists (25). Interestingly, it recently has been hypothesized that fluorescence from PAH aggregates is responsible for broad luminescence in sooting flames (26). In addition, self-assembly of PAH molecules is intriguing from an advanced materials viewpoint, because a well ordered PAH stack may form a novel nanomaterial with exceptionally high charge mobility (27). Charged PAH clusters and isoelectronic species (either charged

Fig. 1. Selected PAH molecules and their dimers. (*A*) Highest occupied molecular orbitals of PAH molecules studied in this work. (*B*) Stacking structures of selected PAH dimer cations and the corresponding binding energy curves. Molecular orbital shapes from *A* are superimposed to aid the visualization of the molecular orbital overlap.

or neutral) will exhibit dramatically different characteristics compared with simple neutral stacked PAHs such as stronger interaction strengths and very different electronic spectroscopy, as we will discuss later.

Results and Discussion

Stability and Abundance of PAH Dimer Cations. Neutral PAH molecule pairs typically form relatively weakly binding van der Waals complexes, with binding energies attributable to dispersion forces of typically 5–7 kcal/mol for molecules of pyrene or perylene size. By contrast, ion-neutral pairs can form more strongly bound dimers through the addition of covalent and electrostatic effects to dispersion interactions. Fig. 1 shows potential energy surfaces of selected cationic PAH dimers as functions of monomer separations [see supporting information (SI) Fig. 3 for more examples]. From the various examples, it is evident that ion-neutral PAH dimers exhibit reasonable chemical stability (15–20 kcal/mol). Because the bonding in such dimers is formed through $\pi-\pi$ molecular orbital overlap, one might assume that proper symmetry matching of the monomers is necessary for strong bond formation. Interestingly, this is not

the case, for two reasons. First, with a proper offset between different monomers, the relevant orbitals still can have reasonable overlap (Fig. 1*B*). Second, important electrostatic effects do not depend on orbital overlap. In fact, all dimers considered here exhibit reasonably strong interactions when the monomers are aligned appropriately. We conclude that dimer formation between cationic and neutral PAH molecules is feasible for various PAH pairs and observe that it is enhanced further by long-range electrostatic steering such as charge–quadrupole interactions.

In the interstellar regions where high-energy radiation is abundant (28), the concentration of PAH cations will be relatively high (23, 29). Significant concentrations of ion-neutral dimers are likely to be present in these regions as well, in equilibrium with the monomers, similar to the PAH neutral-ion equilibrium (23, 30, 31). Because the cation monomer concentration will depend strongly on the flux of ionizing radiation, the dimer concentration also should have some correlation with this flux. Thus, the very strong correlation between ERE and the high-energy radiation environments of the ionization region in Sh 152 (6), the central region of the Red Rectangle, and the H_2 filaments on the surfaces of molecular clouds in the reflection nebula NGC 7023 (18) supports the present hypothesis. Conversely, any ERE caused by dimer cations may show low spatial correlation with emissions from individual PAH molecules. Indeed, the ERE does not correlate with interstellar IR bands at 3.3 and 6.2 μm from the HII region Sh 152 (6), and the blue luminescence and PAH IR emission features from the Red Rectangle nebula (32), which are well ascribed to free PAH molecules (6, 32, 33).

Strong Red Emissions from Closed-Shell PAH Dimer Cations. One very important distinction amongst PAH dimer systems is the spin multiplicity. Excited states of open-shell systems such as perylene$_2{}^+$ with nonzero total spin can undergo nonradiative relaxation to a vibrationally excited ground state (34), significantly decreasing the quantum yield of the luminescence. It is for this reason that open-shell PAH cations have been rejected as possible ERE carriers (e.g., ref. 18). This is not the case for closed-shell systems. Furthermore, because a closed-shell cation such as the phenalenyl ion has lower electron affinity than an open-shell cation of a similar size, the concentration of closed-shell cations will be higher in the interstellar medium. Weilmünster *et al.* (25) have shown that closed-shell PAHs are produced in combustion processes, which are related to the high-energy regions in which interstellar PAHs are likely to be produced (35, 36). Accordingly, strong red emission from interstellar PAH dimer cations may be dominated by closed-shell systems (37).

Table 1 presents the vertical excitation energies for various PAH dimers and monomers. One easily can see that the closed-shell dimers have distinctive, strong visible-to-IR transitions that fall within or close to the ERE envelope (1.4–2.3 eV), whereas dimers with open-shell electronic structure usually have transitions too far to the red of the ERE envelope. In addition, the oscillator strengths for the closed-shell PAH cations are large, satisfying the observational requirement of high luminescence efficiency. Also listed in Table 1 are the transitions for doubly ionized PAHs. These too are closed-shell systems and, for this reason, also have been suggested as possible ERE carriers (18). The entries in Table 1, similar to those reported in ref. 18, show that doubly ionized PAHs do have transitions that fall in the proper wavelength region. However, their oscillator strengths are significantly smaller than those of the closed-shell charged PAH dimers and thus do not meet the high luminescence efficiency observational constraint. Furthermore, many of these also have strong, undetected transitions that fall too far to the blue of the ERE. (Note that similar transitions do not occur in the closed-shell dimer cations.)

Table 1. Calculated vertical excitation energies to the lowest excited electronic states of various ionic PAH systems

System		Multiplicity	Excitation energy, eV	Oscillator strength
Closed-shell dimers	[Pyrene-phenalenyl]$^+$	Singlet	1.65*	0.14[†]
	[Perylene-phenalenyl]$^+$	Singlet	1.25*	0.17[†]
	[Pyrene-naphthanthrenyl]$^+$	Singlet	1.63*	0.06[†]
Open-shell dimers	[Perylene$_2$]$^+$	Doublet	1.03[‡]	0.25[‡]
	[Perylene-pyrene]$^+$	Doublet	0.81[‡]	0.11[‡]
	[Pyrene$_2$]$^+$	Doublet	0.88[‡]	0.17[‡]
Closed-shell dications	Pyrene^{2+}	Singlet	1.30[‡]	0.00[‡]
	Perylene^{2+}	Singlet	1.94[‡]	0.00[‡]

For comparison, the ERE is a broad emission feature extending from ≈1.4 to 2.3 eV, with a maximum at ≈1.8 eV.
*Results are from asymptotically corrected RI-CIS(D).
[†]CIS oscillator strengths.
[‡]Results are from time-dependent density functional theory.

Broad Emission Features. In addition to the fact that charged dimers have electronic transition energies and quantum yields consistent with ERE, from the flexible nature of the dimer bonding curve one should expect that the emission line width will be large. To confirm this proposition, the emission spectrum of [pyrene-phenalenyl]$^+$ system was simulated based on the quantum chemically calculated electronic state surfaces (S$_0$ and S$_1$ in Fig. 2). Fig. 2 also presents the simulated emission features for three different initial vibrational wavepackets, establishing that the emission for this dimer is quite broad. Because the broadness is the result of the loose binding between the monomers, other dimers will exhibit similar profiles, with slightly different centers and widths. With many different dimers, the composite emission spectrum will be very broad with no clear peaks resolved.
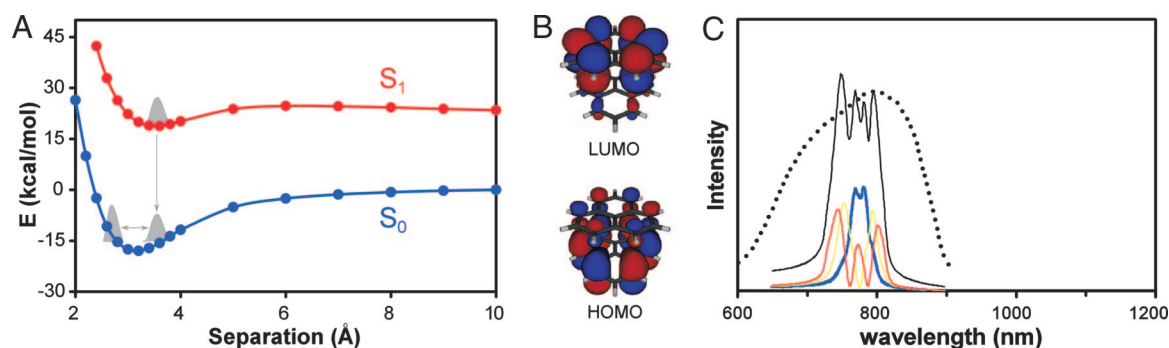
Dependence on the Environment. Other remaining observational features also support the PAH dimer cation hypothesis. First, no ERE has been observed in regions illuminated by relatively low-temperature stars ($T_{eff} < 7,000$ K) (20, 38), which is in keeping with the previous statement that the flux of the ionizing radiation will be a major factor governing the concentration of the PAH ions. The radiation from a low-temperature star does not have an appreciable amount of UV light for the initial ionization step. Furthermore, because different interstellar environments will lead to different distributions in the population of dimer cations, the ERE from various celestial objects will have varying characteristics in terms of peak center and overall broadness.

Conclusions

To summarize, we have shown computationally that various PAH molecules can form cationic dimers with intermediate binding energies between normal van der Waals complexes and chemical bonds. The stacking can occur spontaneously without special substituents or approach directions, as in the case of neutral aromatic molecules (39). Closed-shell cation PAH dimers have optical properties that are markedly different from the monomers with very strong electronic transitions in the red and near-IR regions, as are required to explain the long-standing question of the ERE. In addition, the stability of charged dimers, and the long-range attractions that drive their formation, may represent a route toward formation of the widely observed carbonaceous grains. Indeed, these may be important but previously unrecognized players in soot formation, for which small neutral PAH dimers have been considered but were found to be wanting because of the low van der Waals binding energies (40). The stronger binding energies of the closed-shell charged PAH dimers could resolve this issue. There is a compelling need for additional experimental efforts to obtain gas-phase laboratory spectra of these fascinating species.

Methods

Calculation of Dimer Binding Energies. Binding energies were obtained at various monomer separations. At each separation, the geometry was optimized at the HF/6–31G* level of theory, holding the distance between the monomers fixed (41). The total energy of the geometry thus obtained then is calculated with second-order

Fig. 2. Broad red emission from cationic PAH dimers. (*A*) Ground (S$_0$) and excited (S$_1$) electronic state energies as a function of monomer separation for [pyrene-phenalenyl]$^+$. The emission process involving S$_0$ ← S$_1$ transition also is depicted semiclassically (gray peaks and arrows). (*B* and *C*) It is predominantly charge transfer deexcitation from the acceptor lowest unoccupied molecular orbital (LUMO) to the donor highest occupied molecular orbital (HOMO) (shown in *B*). Wavepacket dynamics on the ground state (as cartooned) leads to the broad calculated line shape presented in *C*. The composite simulated spectrum (black) is obtained by combining emission features from three different vibrational levels on the S$_1$ surface [v = 0 (blue), 1 (yellow), and 2 (red)], assuming that the Frank–Condon factors are the same for the three. The dotted line represents an ERE spectrum reported by Sivan and Perrin (56).

Møller–Plesset perturbation correction (MP2), which is an appropriate level of theory for PAH stacking problems (22). For efficient evaluation of MP2 energies, the resolution-of-the-identity (RI) approximation (sometimes also termed as "density fitting") (42, 43) was adopted in all calculations. The same 6–31G* basis and a corresponding auxiliary basis set (44) were used in these calculations. To correct for basis set superposition error, all energies were counterpoise-corrected so that binding energies should be underestimates. All of the calculations were performed by using the Q-Chem 3.0 package (45).

Calculation of Excited State Surface. Because of the size of these systems, the most accurate (and expensive) electronic structure methods, such as multireference approaches and coupled cluster methods, are not computationally feasible at present. Instead, we carefully have chosen computational protocols to yield reliable results by using low-order many-body methods and density functional theory approaches. Because these methods have known limitations, the most appropriate choice will vary depending on the character of the system studied.

Thus, the results of low-lying electronic transitions of the closed-shell dimer cations were obtained with configuration interaction singles with perturbative doubles corrections [CIS(D)] (46). This method adequately can describe correlation effects on the excitation, while not suffering from self-interaction errors (47) as in time-dependent density functional theory (TDDFT) (48). The self-interaction error-free method becomes especially important for charge-transfer electronic transitions such as the one depicted in Fig. 2. The RI approximation also was adopted to efficiently evaluate the excitation energies, and the same basis functions (6–31G*) were used as in the ground state binding energy calculations. The basis set dependence of the excitation energy was estimated by calculating selected conformations of [pyrene-phenalenyl]$^+$ and [perylene-phenalenyl]$^+$ systems at various monomer separation distances with the larger 6–311+G* basis. (In this additional calculation, the auxiliary basis corresponding to aug-cc-pVTZ (49) set was used.) In all tests, the differences in the excitation energies from using a larger basis set were <0.05 eV.

The RI-CIS(D) energies obtained can be refined further by using asymptotic corrections. In the [pyrene-phenalenyl]$^+$ system, for example, the excitation energy at large separation must be equal to the difference between the ionization energy of pyrene (IE) and the electron affinity of phenalenyl$^+$ (EA). Therefore, the entire excited state surface can be shifted by a constant offset to match the excitation energy at large separation:

$$\omega(R) = \omega^{\text{CIS(D)}}(R) + [(\text{IE} - \text{EA}) - \omega^{\text{CIS(D)}}(R_\infty)]. \quad [1]$$

For accurate assessments of the ionization energies and electron affinities, a combination of MP2 and coupled cluster with perturbative triples correction [CCSD(T)] (50) has been adopted. In this scheme, the absolute energy of a given molecule is obtained at CCSD(T)/6–31G* level of theory and then corrected by ΔE_{basis} as follows:

$$E = E(\text{CCSD(T)}/6\text{–}31\text{G*}) + \Delta E_{\text{basis}} \quad [2]$$

and

$$\Delta E_{\text{basis}} = E(\text{RI-MP2/aug-cc-pVTZ}) - E(\text{RI-MP2/6–31G*}). \quad [3]$$

The quality of the energy value E thus obtained closely follows the quality of the CCSD(T)/aug-cc-pVTZ level. This scheme is conceptually similar to Gaussian-3 theory proposed by Pople and coworkers (51) and is based on observations that ΔE_{basis} is rather insensitive to different levels of theory. The ionization energy is defined as the difference in energies of neutral and ionic species at the neutral geometry, and the electron affinity is defined as the same difference but at the ionic geometry. The geometry of any given species was optimized at RI-MP2 level of theory with cc-pVTZ basis (52).

For open-shell dimers, unrestricted RI-CIS(D) becomes unreliable because of substantial spin contamination in the ground and excited states. Density functional theory is much more resistant to spin-symmetry breaking, and therefore TDDFT was used for the open-shell excited states. The resulting calculations may contain some uncertainties in the excitation energies because of the charge transfer errors mentioned previously. However, because the open-shell systems mainly follow nonradiative deactivation paths (34) as was discussed previously, this possible uncertainty would not impact our explanation of the ERE based on closed-shell cations. For monomer dications, where there is no problem associated with the charge transfer effect, TDDFT was adopted in the calculation of excitation properties.

Simulation of Emission Spectrum. With the excited state curves obtained as above, the emission spectrum was simulated by using a semiclassical approach (53). If the dimer is modeled as a one-dimensional system (as a function of monomer separation), the emission process can be depicted through the progression of a vibrational wavepacket on the model surface. Specifically, the initial vibrational wavepacket $\phi(0)$ is propagated on the ground state surface (S_0) by solving the time-dependent Schrödinger equation with the split-operator method (54). Then the emission spectrum as a function of frequency ω can be obtained from the Fourier transform of the time-correlation function of the propagating wavepacket:

$$I(\omega) = C\omega^3 \int_{-\infty}^{\infty} dt \langle \phi(0)|\phi(t)\rangle e^{i(\omega + \omega_0)t}. \quad [4]$$

Here, ω_0 is the energy of the initial wavepacket on the S_1 surface (53). Because the effect of anharmonicity on low-level vibrations is small, simple Gaussian-type functions with a proper width were used to represent $\phi(0)$.

The emission spectra thus obtained have vibrational structures with ≈ 60 cm^{-1} spacings (equivalent to intermonomer stretching frequencies). In the real emission, these structures will not be observed because the dimers have other low-frequency vibrations [intermonomer bending and shearing (55)] together with extremely small rotational constants with respect to the molecular temperature. Therefore, the envelopes of the vibrational structures were taken as the final spectra.

1. Cohen M, Anderson CM, Cowley A, Coyne GV, Fawley W, Gull TR, Harlan EA, Herbig GH, Holden F, Hudson HS, *et al.* (1975) *Astrophys J* 196:179–189.
2. Witt AN, Schild RE, Kraiman JB (1984) *Astrophys J* 281:708–718.
3. Witt AN, Boroson TA (1990) *Astrophys J* 355:182–189.
4. Furton DG, Witt AN (1992) *Astrophys J* 386:587–603.
5. Gordon KD, Witt AN, Friedmann BC (1998) *Astrophys J* 498:522–540.
6. Darbon S, Zavagno A, Perrin J-M, Savine C, Ducci V, Sivan J-P (2000) *Astron Astrophys* 364:723–731.
7. Perrin J-M, Darbon S, Sivan J-P (1995) *Astron Astrophys* 304:L21–L24.

8. Perrin J-M, Sivan J-P (1992) *Astron Astrophys* 255:271–280.
9. Witt AN, Vijh UP (2004) in *ASP Conference Series 309: Astrophysics of Dust*, eds. Witt AN, Clayton GC, Draine BT (ASP, San Francisco), pp 115–139.
10. Schmidt GD, Cohen M, Margon B (1980) *Astrophys J* 239:L133–L138.
11. Scarrott SM, Watkin S, Miles JR, Sarre PJ (1992) *Mon Not R Astron Soc* 255:11p–16p.
12. d'Hendecourt LB, Léger A, Olofsson G, Schmidt W (1986) *Astron Astrophys* 170:91–96.
13. Wdowiak TJ, Donn B, Nuth JA, Chappelle E, Moore M (1989) *Astrophys J* 336:838–842.
14. Seahra SS, Duley WW (1999) *Astrophys J* 520:719–723.
15. Jones AP, Duley WW, Williams DA (1990) *Q J R Astron Soc* 31:567–582.
16. Witt AN, Schild RE (1988) *Astrophys J* 325:837–845.
17. Witt AN, Gordon KD, Furton DG (1998) *Astrophys J* 501:L111–L115.
18. Witt AN, Gordon KD, Vijh UP, Sell PH, Smith TL, Xie RH (2006) *Astrophys J* 636:303–315.
19. Szomoru A, Guhathakurta P (1998) *Astrophys J* 494:L93–L97.
20. Darbon S, Perrin J-M, Sivan J-P (1999) *Astron Astrophys* 348:990–992.
21. Kira A, Arai S, Imamura M (1971) *J Chem Phys* 54:4890–4895.
22. Small D, Zaitsev V, Jung Y, Rosokha SV, Head-Gordon M, Kochi JK (2004) *J Am Chem Soc* 126:13850–13858.
23. Allamandola LJ, Tielens AG, Barker JR (1989) *Astrophys J Suppl Ser* 71:733–735.
24. Duley WW, Seahra S (1998) *Astrophys J* 507:874–888.
25. Weilmünster P, Keller A, Homann K-H (1999) *Combust Flame* 116:62–83.
26. Miller JH (2005) *Proc Combust Inst* 30:1381–1388.
27. van de Craats AM, Warman JM, Müllen K, Geerts Y, Brand JD (1998) *Adv Mater* 10:36–38.
28. Mathis JS, Mezger PG, Panagia N (1983) *Astron Astrophys* 128:212–229.
29. Allamandola LJ, Tielens AG, Barker JR (1985) *Astrophys J* 290:L25–L28.
30. Bakes ELO, Tielens AGGM (1998) *Astrophys J* 499:258–266.
31. Li A, Draine BT (2001) *Astrophys J* 554:778–802.
32. Vijh UP, Witt AN, Gordon KD (2004) *Astrophys J* 606:L65–L68.
33. Kerr TH, Hurst ME, Miles JR, Sarre PJ (1999) *Mon Not R Astron Soc* 303:446–454.
34. Zhao L, Lian R, Shkrob IA, Crowell RA, Pommeret S, Chronister EL, Liu AD, Trifunac AD (2004) *J Phys Chem A* 108:25–31.
35. Frenklach M, Feigelson ED (1989) *Astrophys J* 341:372–384.
36. Cherchneff I, Barker JR, Tielens AGGM (1992) *Astrophys J* 401:269–287.
37. Hudgins DM, Bauschlicher CW, Allamandola LJ (2001) *Spectrochim Acta A* 57:907–930.
38. Draine BT (2003) *Annu Rev Astron Astrophys* 41:241–289.
39. Sokolov AN, Friscic T, MacGillivray LR (2006) *J Am Chem Soc* 128:2806–2807.
40. Frenklach M (2002) *Phys Chem Chem Phys* 4:2028–2037.
41. Baker J (1997) *J Comput Chem* 18:1079–1095.
42. Vahtras O, Almlöf J, Feyereisen MW (1993) *Chem Phys Lett* 213:514–518.
43. Feyereisen M, Fitzgerald G, Komornicki A (1993) *Chem Phys Lett* 208:359–363.
44. Weigend F, Häser M, Patzelt H, Ahlrichs R (1998) *Chem Phys Lett* 294:143–152.
45. Shao Y, Molnar LF, Jung Y, Kussmann J, Ochsenfeld C, Brown ST, Gilbert ATB, Slipchenko LV, Levchenko SV, O'Neill DP, *et al.* (2006) *Phys Chem Chem Phys* 8:3172–3191.
46. Head-Gordon M, Rico RJ, Oumi M, Lee TJ (1994) *Chem Phys Lett* 219:21–29.
47. Dreuw A, Head-Gordon M (2004) *J Am Chem Soc* 126:4007–4016.
48. Runge E, Gross EKU (1984) *Phys Rev Lett* 52:997–1000.
49. Weigend F, Köhn A, Hättig C (2002) *J Chem Phys* 116:3175–3183.
50. Raghavachari K, Trucks GW, Pople JA, Head-Gordon M (1989) *Chem Phys Lett* 157:479–483.
51. Curtiss LA, Raghavachari K, Redfern PC, Rassolov V, Pople JA (1998) *J Chem Phys* 109:7764–7776.
52. Dunning TH (1989) *J Chem Phys* 90:1007–1023.
53. Heller EJ (1981) *Acc Chem Res* 14:368–375.
54. Leforestier C, Bisseling RH, Cerjan C, Feit MD, Friesner R, Guldberg A, Hammerich A, Jolicard G, Karrlein W, Meyer H-D, *et al.* (1991) *J Comput Phys* 94:59–80.
55. Rapacioli M, Calvo F, Spiegelman F, Joblin C, Wales DJ (2005) *J Phys Chem A* 109:2487–2497.
56. Sivan JP, Perrin JM (1993) *Astrophys J* 404:258–263.